ACS OMEGA

Open Access



http://pubs.acs.org/journal/acsodf

Article

# Superconcentration Strategy Allows Sodium Metal Compatibility in Deep Eutectic Solvents for Sodium-Ion Batteries

An-Sofie Kelchtermans, Dries De Sloovere, Jonas Mercken, Thomas Vranken, Gianfabio Mangione, Bjorn Joos, Willem Vercruysse, Dries Vandamme, Hamid Hamed, Mohammadhosein Safari, Elien Derveaux, Peter Adriaensens, Marlies K. Van Bael, and An Hardy*

Cite This: *ACS Omega* 2024, 9, 42343−42352

Read Online

ACCESS | Metrics & More | Article Recommendations | Supporting Information

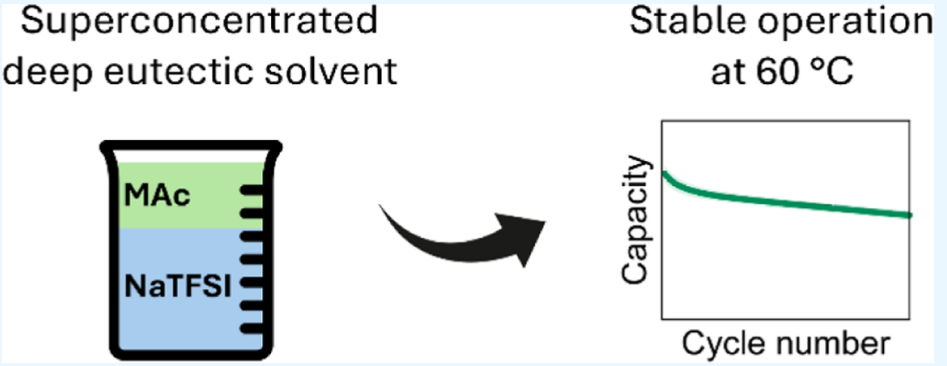


**ABSTRACT:** Sodium-ion batteries (SIBs) are a more sustainable alternative to lithium-ion batteries (LIBs) considering the abundance, global distribution, and low cost of sodium. However, their economic impact remains small compared to LIBs, owing in part to the lag in materials development where significant improvements in energy density and safety remain to be realized. Deep eutectic solvents (DESs) show promise as alternatives to conventional electrolytes in SIBs because of their nonflammable nature. However, their practical application has thus far been hindered by their limited electrochemical stability window. In particular, DESs based on *N*-methylacetamide have thus far been reported not to be stable with sodium metal. In contrast, this work reports a superconcentration strategy where sodium-ion conducting DESs, based on the dissolution of NaFSI in *N*-methylacetamide, are simultaneously stable with sodium metal and Prussian blue as state-of-the-art positive electrode material. At 60 °C, the nonflammable DES outperforms a conventional liquid electrolyte in terms of rate performance and capacity retention. Therefore, these novel DES compositions pave the way for the use of DESs in practical applications with an improved safety and sustainability.

## 1. INTRODUCTION

Since their initial commercialization in 1991, rechargeable lithium-ion batteries (LIBs) have evolved into successful energy storage systems. However, lithium is not considered an abundant element because its relative global abundance is only 0.01%.[1] Furthermore, lithium is unevenly distributed across the globe. Based on the larger abundance (2.83%) and more even global distribution of sodium, along with its low cost and low electrochemical potential (−2.71 V vs standard hydrogen electrode (SHE)), close to that of lithium (−3.04 V vs SHE), sodium-ion batteries (SIBs) are a promising alternative to LIBs.[2−5]

The economic impact of SIBs remains small compared to that of LIBs due to the lack of performant electrode materials and electrolytes.[6−9] While numerous efforts are being undertaken to discover new electrode materials for SIBs, literature reports on the electrolyte remain relatively scarce. The most frequently used SIB electrolyte at the moment is a solution of $NaPF_6$ (∼1 M) in a mixture of alkyl carbonate-based solvents, such as dimethyl carbonate (DMC), diethyl carbonate, ethyl carbonate (EC), or propylene carbonate (PC).[10] An ideal electrolyte should possess the following qualities: a high ionic conductivity, a large thermal stability window, no undesired reactivity toward the electrodes (in a wide temperature range), and a wide electrochemical stability window. Finally, it should be inherently safe and nontoxic. All of these properties are very sensitive to the composition of salt and solvent(s), and to the use of additives in the electrolyte.[11] Additives can also be used to decrease the flammability of conventional electrolytes.[12,13]

**Received:** June 4, 2024
**Revised:** August 21, 2024
**Accepted:** September 6, 2024
**Published:** October 1, 2024

Deep eutectic solvents (DESs) have emerged as a potential electrolyte class in energy storage devices due to their low cost, nontoxic nature, and low vapor pressure.[14,15] DESs and ionic liquids are similar in many ways, including their nonflammability and low vapor pressure. Other benefits of DESs include their low component costs and simplicity of the synthesis process.[16,17] Still, reports on the use of DES electrolytes in SIBs remain scarce. Further, it is challenging to find a DES electrolyte which is simultaneously compatible with both sodium metal and high energy positive electrode materials, such as polyanion compounds, layered oxides, and Prussian blue (PB) analogues.[18−20] De Sloovere et al.[21] reported a series of DESs consisting of sodium bis(trifluoromethanesulfonyl)imide (NaTFSI) in *N*-methylacetamide (MAc). Although an increase in salt concentration significantly increased their anodic stability up to ≈4.65 V vs $Na^+/Na$, even the most concentrated formulations were not compatible with sodium metal. In another report, Xiong et al.[22] dissolved sodium bis(fluorosulfonyl)imide (NaFSI) in 1,2-dimethylimidazole to obtain a DES with excellent compatibility toward sodium metal. However, its electrochemical stability window remained limited to 3.2 V, as determined from LSV measurements at 100 mV $s^{-1}$. The DES reported by Chen et al.[23] consists of $NaClO_4$, 1,3,2-dioxathiolane-2,2-dioxide (DTD) and succinonitrile, has a room temperature conductivity of 2.86 mS $cm^{-1}$ and has excellent stability toward $Na_3V_2(PO_4)_3$, hard carbon, and sodium metal. Here, the formation of hydrogen bonds between DTD and succinonitrile enables the latter's compatibility with sodium metal. However, the high cost of DTD may limit this DES' commercial viability. In a similar approach, the electrochemical stability window of water was extended to 3.41 V by the dissolution of $NaClO_4$ and succinonitrile, essentially creating a water-locked eutectic electrolyte.[24]

This work reports a new series of sodium-based DES electrolytes, where a superconcentration strategy is used for the dissolution of NaFSI in MAc. The coordination structure of these DESs was studied by FTIR, Raman, and NMR spectroscopy, revealing the importance of ionic interactions on the functional properties of these DESs. In particular, the coordination structure has a pronounced effect on the ionic conductivity, anodic stability limit, and compatibility toward sodium metal. In PB/sodium cells, the most concentrated DES outperformed a conventional electrolyte in terms of rate performance and electrochemical stability. Compared to previously reported DESs, the compositions reported in this work offer an improved electrochemical stability without the need for expensive hydrogen bond donors/acceptors. As such, this work brings the use of DESs in safe and sustainable applications a step closer.

## 2. METHODS

**2.1. Chemicals.** Sodium bis(fluorosulfonyl)imide (NaFSI, 99.9%, Solvionic) was utilized as received. After purchasing *N*-methylacetamide (MAc, ≥ 99%, Sigma-Aldrich), it was dried for 72 h at 45 °C using molecular sieves (3 Å, 4−8 mesh, Acros). The chemicals were stored in a glovebox filled with argon (Sylatech, $H_2O$ < 0.1 ppm, $O_2$ < 0.1 ppm).

**2.2. Preparation of the DESs.** Appropriate amounts of NaFSI and MAc were mixed at 50 °C in an argon-filled glovebox until a transparent mixture was obtained.

**2.3. Physicochemical Characterization.** Fourier transform infrared spectroscopy (FTIR, PerkinElmer Frontier, 16 scans, 4000−400 $cm^{-1}$ scan range, 4 $cm^{-1}$ resolution) was used to examine the DES coordination structure. The measurements were carried out using the MIRacle single reflection ATR. Thermogravimetric analysis (TGA, TA Instruments Q600) was used to study the thermal decomposition of the electrolytes by heating 2−8 mg of the samples (10 °C $min^{-1}$ to 600 °C, $N_2$ flow). A differential scanning calorimeter (DSC, TA Instruments Q200) was used for the calorimetric studies. The samples were heated from −90 to 60 °C at 10 °C $min^{-1}$ while being sealed in aluminum hermetic pans and subjected to a 50 mL $min^{-1}$ nitrogen flow. Using an Anton Paar MCR102 rheometer, the viscosity of the DES was determined at a shear rate of 100 $s^{-1}$. On a Jeol ECZ400R spectrometer, NMR spectra were obtained at 399.8, 376.2, and 105.7 MHz for $^1H$, $^{19}F$, and $^{23}Na$ spectra, respectively, using a 5 mm Royal HFX probe at RT. Acquisition parameters used were (i) for $^1H$ NMR: a spectral width of 6 kHz (15 ppm), a 90° pulse length of 6.8 $\mu$s, an acquisition time of 2.2 s, a recycle delay time of 12 s and 64 accumulations; (ii) for $^{19}F$ NMR: a spectral width of 151.5 kHz (400 ppm), a 90° pulse length of 7.9 $\mu$s, an acquisition time of 0.7 s, a recycle delay time of 10 s and 64 accumulations; and (iii) for $^{23}Na$-NMR: a spectral width of 64.1 kHz (600 ppm), a 90° pulse length of 22 $\mu$s, an acquisition of 0.2 s, a recycle delay time of 10 s and 200 accumulations. Raman spectra were collected using a Renishaw InVia Qontor Confocal Raman Microscope with a 10× objective and a 785 nm excitation wavelength to give a laser spot volume of approximately 400 $\mu m^3$. The measurements were performed at room temperature in continuous scan mode (SynchroScan) with an exposure time of 10 s, 3 accumulations, 100% laser power, and a 1200 L/mm grating. The obtained spectra were analyzed using Renishaw WIRE 5.6 software and cosmic rays were removed when present.

**2.4. Electrochemical Characterization.** A Mettler Toledo FiveEasy Plus conductometer was used to measure the ionic conductivity of the DESs while the samples were submerged in a thermostatic bath that ranged in temperature from −10 to 60 °C. Using a three-electrode setup consisting of a stainless steel working electrode, a sodium metal counter electrode, and a sodium metal reference electrode, linear sweep voltammetry (LSV, Bio-Logic, VMP3) was used to assess the electrochemical stability window of the DESs. A glass fiber disk (18 mm in diameter and 1.55 mm in thickness, EL-CELL) soaked with the DES under investigation served as a separator between the electrodes. The working electrode potential was swept from the open-circuit potential (OCP) to 5 V vs $Na^+/Na$ in the anodic scan, and to −1 V vs $Na^+/Na$ in the cathodic scan, with a scan rate of 1 mV $s^{-1}$. The electrochemical compatibility of the DESs with sodium metal was tested by electrochemical impedance spectroscopy (EIS) in a symmetric Na/DES/Na cell. To execute EIS (Bio-Logic, SP-300), the OCP was perturbed using an alternating sinusoidal potential with an amplitude of 10 mV over a frequency range of 10 kHz to 100 mHz. The long-term stability between the DES electrolyte and Na metal was assessed by a stripping/plating test in a symmetric Na/DES/Na cell, where the DES was impregnated in a glass fiber separator (19 mm diameter, 0.26 mm thickness, purchased from EL-CELL). Here, a current of 0.05 mA $cm^{-2}$ was applied in alternating directions (30 min per half cycle, BioLogic SP-300).

Electrodes were formulated with 85 wt % PB ($Na_{0.61}Fe[Fe(CN)_6]_{0.94}$, NEI corporation), 10 wt % carbon black (C65, Imerys), and 5 wt % PVDF (1.35 wt % in *N*-methyl


https://doi.org/10.1021/acsomega.4c02896
ACS Omega 2024, 9, 42343−42352

Table 1. Molality (molar Amount of NaFSI Divided by the Weight of MAc), Molar Ratio, Anodic Stability Limit, and Ionic Conductivity at 0, 20, and 60 °C of the DESs[a]

| sample | molality NaFSI (m) | [NaFSI]/[MAc] molar ratio | anodic stability limit vs $Na^+/Na$ (V) | ionic conductivity (mS $cm^{-1}$) | | |
|---|---|---|---|---|---|---|
| | | | | 0 °C | 20 °C | 60 °C |
| DES-1 | 13.7 | 1:1 | ≈4.0 | 0.00343 | 0.0561 | 3.65 |
| DES-2 | 6.84 | 1:2 | ≈3.7 | 0.141 | 0.820 | 8.73 |
| DES-3 | 4.56 | 1:3 | | 0.319 | 3.35 | 15.6 |
| DES-4 | 3.42 | 1:4 | | 0.754 | 4.46 | 18.0 |
| DES-5 | 2.74 | 1:5 | | 0.901 | 5.31 | 17.1 |
| DES-6 | 1.95 | 1:7 | | 1.23 | 6.50 | 18.0 |
| DES-7 | 1.52 | 1:9 | | 1.25 | 6.58 | 17.7 |

[a]The anodic stability limit of less concentrated DESs could not be measured due to their reactivity with Na metal (indicated by a dash).

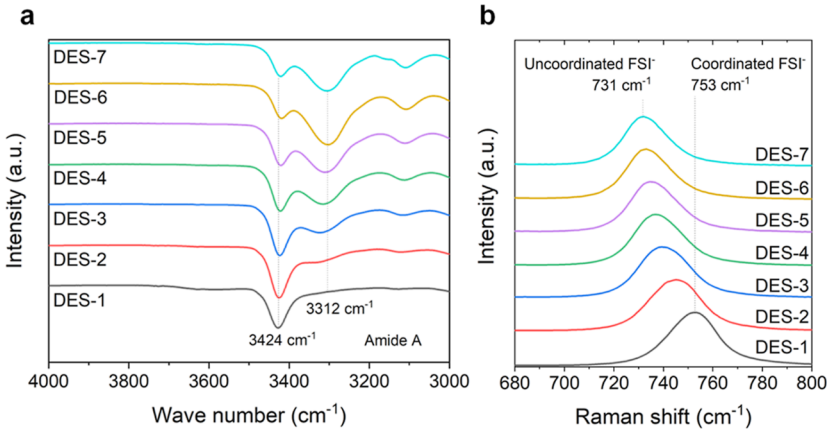


**Figure 1.** MAc—MAc hydrogen bonds are replaced by ionic interactions when the salt concentration increases. (a) FTIR and (b) Raman spectra of the investigated set of DESs with normalized peak intensities.

pyrrolidone, Roth Chemicals), using a ball mill (Retsch Emax, 500 rpm, 30 min, 5 × 1 cm zirconia balls). Next, the resulting slurry was tape casted on aluminum foil with a blade height of 100 $\mu$m, dried overnight in air at 60 °C, followed by drying under vacuum in a Büchi glass oven B-585 at 110 °C for 15 h. PB/Na cells were assembled in an argon-filled glovebox. A thin glass fiber (EL-CELL, 19 mm diameter, 0.26 mm thickness) soaked with the DES electrolyte (120 $\mu$L) was used as separator. Prior to galvanostatic cycling (2.2−4 V vs $Na^+/Na$), all coin cells underwent a 16 h OCP period.

## 3. RESULTS AND DISCUSSION

Seven NaFSI/MAc-based DES electrolytes with different NaFSI concentrations were prepared. Table 1 summarizes their exact compositions, their ionic conductivity at 0, 20, and 60 °C, and their anodic stability limit. Further details are given in Supporting Information. As both DES-1 and DES-2 contain a higher mass of NaFSI than MAc, we consider these to be superconcentrated DESs.

**3.1. Coordination Structure.** A previous study established the importance of the solution coordination structure for the electrochemical properties of DES electrolytes consisting of NaTFSI and MAc.[21] At high salt concentrations, MAc−MAc hydrogen bonds are broken in favor of strong ionic interactions between MAc, $Na^+$, and $TFSI^-$, giving rise to a shift in the energy levels of the molecular orbitals, and ultimately to an increased anodic stability. Given the critical role of the solution coordination structure, the chemical interactions in the NaFSI-based DESs presented in this paper were thoroughly characterized using FTIR, Raman, and NMR spectroscopy.

The MAc coordination environment can be readily studied using FTIR spectroscopy (Figure 1a). When its N−H moiety is involved in hydrogen bonds, the amide A band is located around 3312 $cm^{-1}$. The amide A band will shift toward higher wave numbers as the hydrogen bonds are replaced by ionic interactions. In our set of DESs, the amide A band at 3424 $cm^{-1}$ becomes more intense compared to the band at 3312 $cm^{-1}$ as the salt concentration increases. This suggests that in highly concentrated DESs, ionic interactions replace MAc−MAc hydrogen bonds.[25] The complete FT-IR spectra are given in Figure S1.[26−28] Further information on the solution coordination structure was gathered with Raman spectroscopy (Figures 1b, S2). This technique is particularly useful for assessing the coordination environment of the $FSI^-$ anion, as the bands in the 700−770 $cm^{-1}$ range are characteristic for its S−N stretching modes. The most relevant Raman peaks are described in Table S2. In the Raman spectra of DES-7 (which has the lowest salt content), the band at 731 $cm^{-1}$ corresponds to uncoordinated $FSI^-$ anions. With increasing NaFSI concentration, the $FSI^-$ bands shift to higher Raman shifts, indicating that the $FSI^-$ anions experience more pronounced ionic interactions.[29]

The nature of the ionic interactions in the DESs was further investigated with NMR spectroscopy (Figure 2). The $^1H$ NMR spectra (Figure 2a) indicate that as the concentration of NaFSI increases, there is a significant upfield shift of the MAc NH signal from 8.2 to 6.7 ppm. Additionally, there is an upfield shift for both the MAc $CH_3-C{=}O$ methyl group (from 3.1 to 2.9 ppm) and $NH-CH_3$ methyl group (from 2.3 to 2.15 ppm).


https://doi.org/10.1021/acsomega.4c02896
ACS Omega 2024, 9, 42343−42352

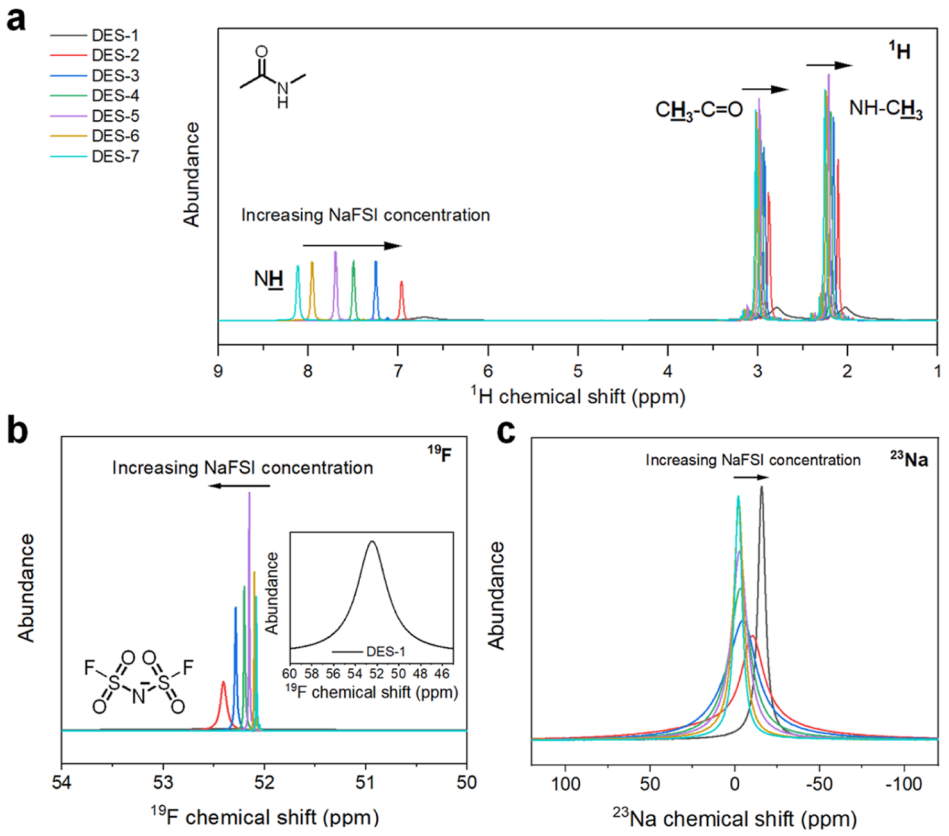


**Figure 2.** (a) $^{1}$H, (b) $^{19}$F, and (c) $^{23}$Na NMR spectra of the set of DES electrolytes. Increasing the NaFSI concentration leads to upfield shifts of the $^{1}$H and $^{23}$Na NMR signals, and to a downfield shift of the $^{19}$F NMR signals. In the $^{19}$F spectra, DES-1 is placed as a zoomed insert.

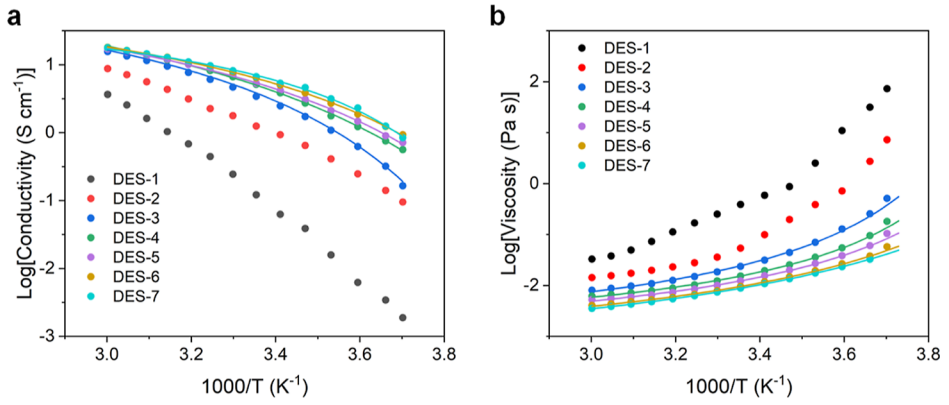


**Figure 3.** Plot of the (a) ionic conductivity (b) viscosity of the DES electrolytes as a function of temperature. The dots represent the data points, and the full lines represent the fits to the VTF equations. For DES-1 and DES-2, neither the ionic conductivity nor the viscosity could be reliably fitted.

As intermolecular hydrogen bonding causes a downfield shift of the NMR signal, the upfield shift of the signals indicates an increase in ionic interaction. Moreover, a significant increase in signal broadening is observed for DES-2 and DES-1, indicating a reduced freedom of MAc mobility. The signals in the $^{19}$F NMR spectra (Figure 2b) show a downfield shift as the concentration of NaFSI increases, suggesting that the $FSI^{-}$ ions take part in the ionic interactions. Also here, severe signal broadening is observed for DES-2 and DES-1, indicating a reduced freedom of mobility for the $FSI^{-}$ ions. The $^{23}$Na NMR spectra (Figure 2c) show that an increased NaFSI concentration leads to an upfield shift and signal broadening, suggesting that the $Na^{+}$ ions are actively involved in the ionic interactions as well. The signal broadening indicates a decreased degree of $Na^{+}$ ion mobility. Whereas the most pronounced upfield shift is observed for DES-1, the signal is significantly less broad than is the case for less concentrated DESs. Whereas this may suggest an increased $Na^{+}$ ion mobility in this sample (and therefore, an increased sodium ion transference number), one should note that the line width is also determined by the exchange rate between chemical sites.[30] In any case, the narrow signal suggests that the $Na^{+}$-$TFSI^{-}$-MAc complexes formed in this DES are significantly different from those formed in less concentrated DESs. The presence of such complexes may allow to achieve a combination of high ionic conductivity and broad electrochemical stability which is


https://doi.org/10.1021/acsomega.4c02896
ACS Omega 2024, 9, 42343−42352

not possible for less concentrated DESs, where there is always a trade-off between both factors.

The spectroscopy results presented above indicate that an increase in NaFSI concentration leads to the breakage of MAc−MAc hydrogen bonds. Instead, strong ionic interactions lead to the formation of $Na^+$-$TFSI^-$-MAc complexes. As shown in our previous work,[21] this may cause a significant shift in the energy levels of the molecular orbitals, which ultimately affects the electrochemical stability window of the DES electrolytes. As such, an increase in salt concentration may allow to extend the anodic stability to higher potentials, while simultaneously allowing compatibility with sodium metal. This will be studied in detail in the following sections.

**3.2. Ionic Conductivity and Viscosity.** The ionic conductivity and viscosity values of the investigated DESs were measured in a broad temperature range (between −3 and 60 °C, Figure 3). Overall, the ionic conductivity decreases and the viscosity increases with increasing salt concentration, in line with the NMR spectroscopy results. For the less concentrated DESs, i.e. DES-3 to DES-7, the variation of ionic conductivity and viscosity can be described by the Vogel−Tammann−Fulcher (VTF) equations

$$\sigma = \sigma_0 e^{-B/T-T_0} \quad (1)$$

$$\eta = \eta_0 e^{B'/T-T_0} \quad (2)$$

In eqs 1 and 2, the conductivity and viscosity at infinite temperature are represented by the pre-exponential components $\sigma_0$ and $\eta_0$, respectively. $B$, $B'$, and $T_0$ describe the temperature dependence. For DES-3 to DES-7, these parameters were fitted to the VTF eq (Table 2). However,

**Table 2. Ionic Conductivity for the DES Electrolytes Combined with VTF Model Parameters**

| sample | conductivity | | | viscosity | | |
|---|---|---|---|---|---|---|
| | $\sigma_0$ (mS cm$^{-1}$) | $B$ (K) | $T_0$ (K) | $\eta_0$ (Pa s) | $B'$ (K) | $T_0$ (K) |
| DES-1 | | | | | | |
| DES-2 | | | | | | |
| DES-3 | 278 | 127 | 230 | 0.0493 | 85 | 237 |
| DES-4 | 460 | 167 | 213 | 0.0519 | 7 | 236 |
| DES-5 | 270 | 137 | 217 | 0.0467 | 77 | 231 |
| DES-6 | 185 | 113 | 22 | 0.0377 | 98 | 220 |
| DES-7 | 81 | 65 | 237 | 0.0323 | 11 | 213 |

the ionic conductivity and viscosity of DES-1 and DES-2 could not be reliably fitted to these equations, meaning that they cannot be accurately described by the VTF equations in the investigated temperature range. Particularly for DES-1, the variation with temperature is more pronounced than for the other DESs, which may be related to the decreased peak width observed in $^{23}$Na NMR (Figure 2c). At 20 °C, DES-1 has an ionic conductivity of 0.0561 mS cm$^{-1}$, which increases to 3.65 mS cm$^{-1}$ at 60 °C. Therefore, this DES is more suitable for operation at higher temperatures. In contrast, DES-2 has an ionic conductivity of 0.820 mS cm$^{-1}$ at 20 °C, implying that this DES may be more suited for room temperature operation.

**3.3. Thermal Stability.** The thermal stability of the set of DESs was studied with thermogravimetric analysis (TGA, Figure S3). The onset temperature for DES degradation increases with increasing NaFSI concentration, up to ≈150 °C for DES-1, as compared to ≈50 °C for DES-7, most probably due to the stronger ionic interactions in more concentrated DESs. As such, the thermal stability of the more concentrated DESs (i.e., DES-1 to DES-4) exceeds that of a conventional liquid electrolyte (i.e., 1 M $NaClO_4$ in EC/PC). After an initial degradation step, the mass loss profiles of all DESs reach a plateau. A comparison of the experimental residual masses with the theoretical values reveals that this plateau corresponds to the composition where all MAc has evaporated. At higher temperatures, the salt is degraded, similarly to previously investigated DES compositions.[21,31] The glass transition temperatures of the DESs were investigated with DSC (Figure S4).

The flammability of the most concentrated DESs was assessed by means of a combustion test where a drop of DES was exposed to a torch. Neither DES-1 nor DES-2 could be ignited after 5−6 s of flame contact, even after repeated flame contact (Supporting Information). We presume that the strong ionic interactions in these samples cause a low vapor pressure, which implies that no combustible vapor can be formed. The nonflammable nature of these DESs means that they facilitate the safety of battery operation.

**3.4. Compatibility with Sodium Metal.** A wide electrochemical stability window is a crucial functional property of any electrolyte. It was previously reported that sodium metal reacts quickly with MAc, but that this reactivity diminishes as more salt is dissolved into the DES.[21] As such, the reactivity of MAc molecules depends on their coordination environment: when involved in an ionic bond, the reactivity is much lower than when involved in a hydrogen bond. The spectroscopy results in this paper also indicate a changing MAc coordination environment with increasing salt concentration. Therefore, we expect a similar behavior for the DESs reported in the paper at hand. A piece of sodium (∼20 mg) was added to each DES composition (1 mL), and the sodium dissolution (and corresponding formation of precipitates) was visually observed throughout time (Figure S5). The sodium metal quickly dissolved in the less concentrated DES compositions: after 5 days, it was totally dissolved in DES-5, DES-6, and DES-7, and partially dissolved in DES-4. The sodium metal was noticeably less soluble in the more concentrated DESs (DES-1, DES-2, and DES-3). Therefore, the stability of these DESs was more thoroughly investigated in Na/DES/Na symmetrical cells at room temperature, which were subjected to EIS over regular time intervals (Figure S6). The Nyquist plots show a lower charge transfer resistance ($R_{ct}$) with increasing NaFSI concentration, implying that less resistive degradation layers are formed on the sodium metal surface. As implied by the stability of the $R_{ct}$ over time, these layers are most robust for DES-1 and DES-2. The continuously increasing $R_{ct}$ of the Na/DES-3/Na cells implies that this DES is continuously degraded, indicating a poor compatibility between DES-3 and sodium metal. Therefore, this DES was discarded from further investigation.

The previous results indicate that DES-1 and DES-2 are compatible with sodium metal at room temperature. As DES-1 may be more suitable for operation at higher temperatures, the stability of symmetrical Na/DES/Na cells was also investigated at 60 °C by means of galvanostatic plating/stripping tests. In these tests, a current of 0.05 mA cm$^{-2}$ was applied with a half cycle capacity of 0.025 mA cm$^{-2}$ (i.e., 30 min per half cycle). This process was repeated for 450 h, with a stable voltage profile without short circuit (Figure 4). A slight increase of polarization is observed over time. EIS measurements before



https://doi.org/10.1021/acsomega.4c02896
ACS Omega 2024, 9, 42343−42352

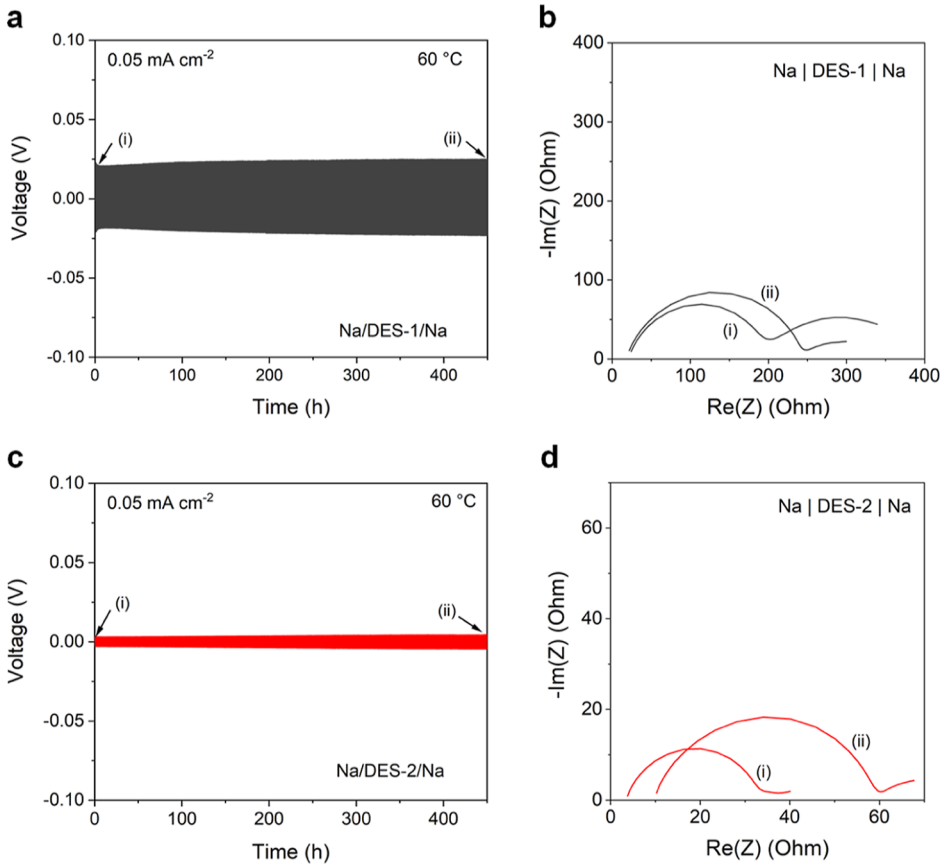


**Figure 4.** (a) Galvanostatic stripping/plating curves of Na/DES-1/Na cells at 60 °C. A current of 0.05 mA $cm^{-2}$ was applied for 30 min until the polarity was reversed. (b) Corresponding Nyquist plot representation of the impedance spectra of the Na/DES-1/Na cells before and after the stripping/plating test. (c) Galvanostatic stripping/plating curves of Na/DES-2/Na cells at 60 °C. A current of 0.05 mA $cm^{-2}$ was applied for 30 min until the polarity was reversed. (d) Corresponding Nyquist plot representation of the impedance spectra of the Na/DES-2/Na cells before and after the stripping/plating test.

and after the stripping/plating tests show an increasing $R_{ct}$, indicating the formation of a resistive degradation film. Still, these results indicate that these two DES electrolytes have a promising compatibility with sodium metal, in contrast with previously reported MAc-based DESs.[21]

**3.5. Anodic Stability.** Using a three-electrode setup consisting of a stainless steel working electrode, a sodium metal counter electrode, and a sodium metal reference electrode, the anodic stability limits of DES-1 and DES-2 were evaluated with linear sweep voltammetry (LSV). DES-1, with its higher salt concentration, has a slightly higher anodic stability limit than DES-2 (Figure 5). This is in line with the observation that increasing salt concentrations lead to the replacement of MAc−MAc hydrogen bonds with strong ionic interactions between $Na^+$, $FSI^-$ and MAc. The related shift in molecular orbital energy levels shifts the anodic stability of the electrolytes. Both DESs are potentially compatible with positive electrode materials operating up to 4 V vs $Na^+$/Na. The cathodic LSVs of similar three-electrode cells indicate that both DES-1 and DES-2 are reduced at low voltages (Figure S7).

**3.6. Application in Supercapacitors and in SIBs.** The functional characterization presented above suggests that the set of DESs may be used as electrolyte for supercapacitors. This is further elaborated on in the (Figures S8−S12).[32−39] Additionally, both DES-1 and DES-2 are electrochemically compatible with both sodium metal and with positive electrode

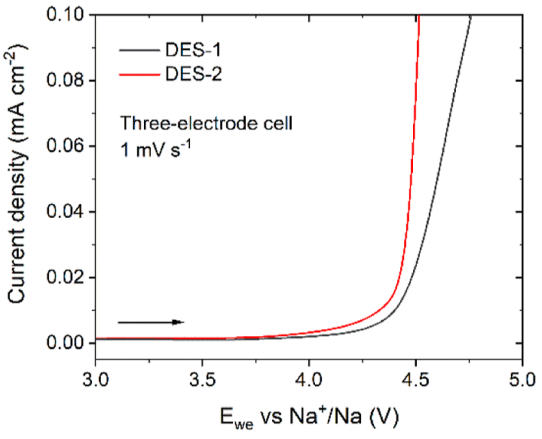


**Figure 5.** With an increase in NaFSI concentration, the anodic stability limit of the DES compositions increases. LSV of DES-1 and DES-2 impregnated in a glass fiber separator and placed between a stainless steel working electrode, a sodium metal reference electrode, and sodium metal counter electrode in a three-electrode setup. The potential at the working electrode was swept from the OCP to 5 V vs $Na^+$/Na at a scan rate of 1 mV $s^{-1}$ at room temperature.

materials operating at up to ∼4 V vs $Na^+$/Na. PB, a transition metal hexacyanoferrate with an open framework structure, is an excellent example of the latter. Operating between 2.2 and 4 V vs $Na^+$/Na, it has a theoretical capacity of ∼170 mAh $g^{-1}$.[40] As


https://doi.org/10.1021/acsomega.4c02896
ACS Omega 2024, 9, 42343−42352

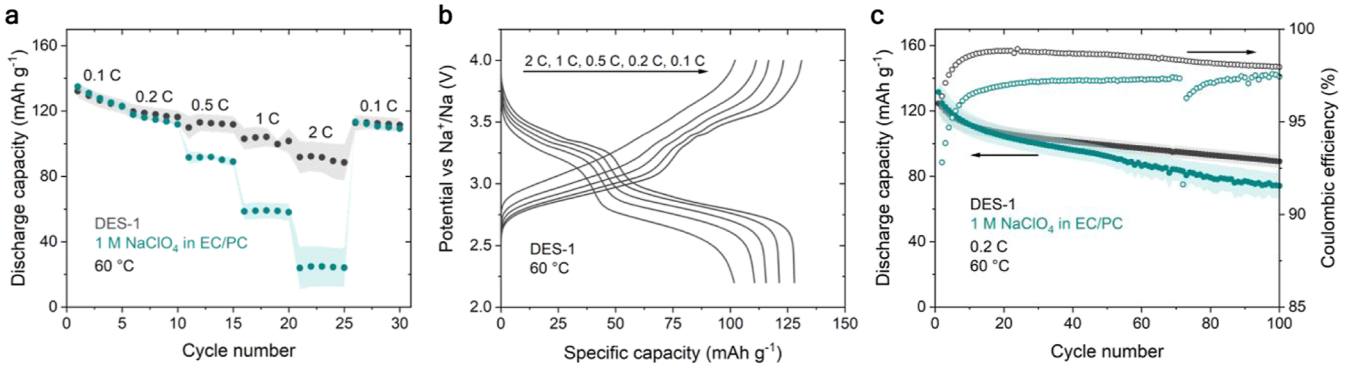


**Figure 6.** (a) Rate performance and (b) corresponding charge/discharge curves of PB/Na cells containing DES-1 or 1 M $NaClO_4$ in EC/PC as liquid electrolyte. (c) Cycle stability test of PB/Na cells performed at 0.2 C. All electrochemical tests were performed in the voltage window of 2.2−4 V vs $Na^+$/Na and at 60 °C. The average active mass loading of the PB electrode was 1.2 mg $cm^{-2}$, which corresponds to 0.204 mAh $cm^{-2}$ assuming a theoretical capacity of 170 mAh $g^{-1}$. The shaded areas indicate the standard deviation according to three separate measurements.

stated above, the limited ionic conductivity of DES-1 at room temperature renders it more suitable for use at higher temperatures, whereas DES-2's higher conductivity may enable its use at room temperature. Therefore, both PB/DES-1/Na and PB/DES-2/Na cells were constructed, where the former were tested at 60 °C and the latter were tested at room temperature. For comparison, similar cells with a conventional electrolyte were also constructed.

At room temperature, the use of DES-2 as electrolyte does not lead to an improved electrochemical performance compared to the conventional electrolyte (Figure S13).[11] However, at 60 °C, PB/DES-1/Na cells perform significantly better than conventional cells. At rates of 0.1 and 0.2 C, both types of cell deliver a similar discharge capacity (Figure 6a). The cells containing DES-1 deliver 112, 102, and 89 mAh $g^{-1}$ at 0.5, 1, and 2 C, respectively. This is considerably higher than the capacities of 89, 58, and 24 mAh $g^{-1}$ delivered by the conventional cell at the same rates. The low polarization during galvanostatic cycling is evident from the galvanostatic charge/discharge curves (Figure 6b). After 100 cycles at 0.2 C, the DES-based cells retain 72% of their initial capacity of 125 mAh $g^{-1}$, as compared to 56% and 131 mAh $g^{-1}$ for the conventional cells (Figure 6c). The improved capacity retention of the DES-based cells is also related to an increased Coulombic efficiency throughout the entire cycling process. We attribute the superior electrochemical performance of DES-1 at 60 °C to its combination of sufficient ionic conductivity with high electrochemical stability. Using conventional, carbonate-based electrolytes without additives leads to a continuously increasing resistance during cell operation.[41] This is also evident from the low Coulombic efficiency observed for 1 M $NaClO_4$ in EC/PC in our case. We surmise that the use of DES-1 as electrolyte leads to the formation of most robust, conductive degradation layers during cell operation, thereby allowing an improved electrochemical operation in terms of rate performance and cycle stability. In lithium-based DESs, higher temperatures during cell operation can lead to a higher fluoride content in the SEI.[42] A similar mechanism may be at play in the case at hand. As such, this type of DES holds promise as functional electrolyte, albeit only at higher operating temperatures. This is relevant for large-scale energy storage, where batteries can be subjected to high temperatures because of the climate, and because of the heat generated during high power operation.

## 4. CONCLUSIONS

Nonflammable DESs are promising alternatives for highly flammable conventional electrolytes in applications where the primary consideration is safety, such as SIBs in stationary applications. However, the number of reported DES electrolytes for SIBs has remained limited thus far, and the reported compositions have limited stability or rely on the use of expensive hydrogen bond donors/acceptors. In contrast, this work reports a series of stable DESs, based on the dissolution of NaFSI in MAc, with an electrochemical performance exceeding that of a conventional carbonate-based electrolyte at 60 °C. PB/sodium cells containing a DES electrolyte deliver 89 mAh $g^{-1}$ at a rate of 2 C, whereas this value drops to 24 mAh $g^{-1}$ for a conventional electrolyte. The former cells retain 72% of their initial capacity of 125 mAh $g^{-1}$ after 100 cycles at 0.2 C (as compared to 56% and 131 mAh $g^{-1}$ for the conventional electrolyte). The superior DES compatibility with both PB and sodium metal is achieved by a superconcentration strategy, where intermolecular hydrogen bonds are replaced by ionic interactions. These strong interactions further result in an improved thermal stability and lower flammability as compared to conventional carbonate-based electrolytes. The improved stability of this set of DESs is a step forward for the practical use of DESs as electrolytes in safe and sustainable SIBs.

## ■ ASSOCIATED CONTENT

### Supporting Information

The Supporting Information is available free of charge at https://pubs.acs.org/doi/10.1021/acsomega.4c02896.

Flammability DES-1. Flammability DES-2 (MP4)

Additional experimental details, FTIR spectra, Raman spectra, ionic conductivity, thermograms, DSC curves, photographs, Nyquist plots, LSV curves, supercapacitor characterization, galvanostatic cycling data (PDF)

## ■ AUTHOR INFORMATION

### Corresponding Author

**An Hardy** − *Institute for Materials Research (imec-imomec), Design and Synthesis of Inorganic Materials (DESINe), Hasselt University, Hasselt B-3500, Belgium; Energyville, imo-imomec, Genk B-3600, Belgium;* orcid.org/0000-0002-5012-0356; Email: an.hardy@uhasselt.be



https://doi.org/10.1021/acsomega.4c02896
*ACS Omega* 2024, 9, 42343−42352

### Authors

**An-Sofie Kelchtermans** − *Institute for Materials Research (imec-imomec), Design and Synthesis of Inorganic Materials (DESINe), Hasselt University, Hasselt B-3500, Belgium; Energyville, imo-imomec, Genk B-3600, Belgium;* orcid.org/0000-0001-6957-2216

**Dries De Sloovere** − *Institute for Materials Research (imec-imomec), Design and Synthesis of Inorganic Materials (DESINe), Hasselt University, Hasselt B-3500, Belgium; Energyville, imo-imomec, Genk B-3600, Belgium;* orcid.org/0000-0001-9358-1278

**Jonas Mercken** − *Institute for Materials Research (imec-imomec), Design and Synthesis of Inorganic Materials (DESINe), Hasselt University, Hasselt B-3500, Belgium; Energyville, imo-imomec, Genk B-3600, Belgium*

**Thomas Vranken** − *Institute for Materials Research (imec-imomec), Design and Synthesis of Inorganic Materials (DESINe), Hasselt University, Hasselt B-3500, Belgium; Energyville, imo-imomec, Genk B-3600, Belgium*

**Gianfabio Mangione** − *Institute for Materials Research (imec-imomec), Design and Synthesis of Inorganic Materials (DESINe), Hasselt University, Hasselt B-3500, Belgium*

**Bjorn Joos** − *Institute for Materials Research (imec-imomec), Design and Synthesis of Inorganic Materials (DESINe), Hasselt University, Hasselt B-3500, Belgium; Energyville, imo-imomec, Genk B-3600, Belgium;* orcid.org/0000-0001-8697-8330

**Willem Vercruysse** − *Institute for Materials Research (imec-imomec), Design and Synthesis of Inorganic Materials (DESINe), Hasselt University, Hasselt B-3500, Belgium;* orcid.org/0000-0002-0838-1616

**Dries Vandamme** − *Institute for Materials Research (imec-imomec), Design and Synthesis of Inorganic Materials (DESINe), Hasselt University, Hasselt B-3500, Belgium;* orcid.org/0000-0003-0941-2434

**Hamid Hamed** − *Institute for Materials Research (imec-imomec), Design and Synthesis of Inorganic Materials (DESINe), Hasselt University, Hasselt B-3500, Belgium; Energyville, imo-imomec, Genk B-3600, Belgium*

**Mohammadhosein Safari** − *Institute for Materials Research (imec-imomec), Design and Synthesis of Inorganic Materials (DESINe), Hasselt University, Hasselt B-3500, Belgium; Energyville, imo-imomec, Genk B-3600, Belgium*

**Elien Derveaux** − *Institute for Materials Research (imec-imomec), Design and Synthesis of Inorganic Materials (DESINe), Hasselt University, Hasselt B-3500, Belgium*

**Peter Adriaensens** − *Institute for Materials Research (imec-imomec), Design and Synthesis of Inorganic Materials (DESINe), Hasselt University, Hasselt B-3500, Belgium*

**Marlies K. Van Bael** − *Institute for Materials Research (imec-imomec), Design and Synthesis of Inorganic Materials (DESINe), Hasselt University, Hasselt B-3500, Belgium; Energyville, imo-imomec, Genk B-3600, Belgium;* orcid.org/0000-0002-5516-7962

Complete contact information is available at: https://pubs.acs.org/10.1021/acsomega.4c02896


### Author Contributions

An-Sofie Kelchtermans: Conceptualization, Methodology, Validation, Formal analysis, Investigation, Writing - original draft, Writing - review and editing, Visualization. Dries De Sloovere: Conceptualization, Methodology, Validation, Investigation, Writing - original draft, Writing - review and editing, Supervision. Jonas Mercken: Methodology (DSC, electrode formulation), Validation, Investigation, Writing - original draft, Writing - review and editing. Thomas Vranken: Methodology (EIS, Rheology), Validation, Writing - original draft, Writing - review and editing. Gianfabio Mangione: Methodology (Raman), Validation, Investigation, Writing - original draft, Writing - review and editing. Bjorn Joos: Conceptualization, Methodology, Validation, Writing - original draft, Writing - review and editing, Supervision, Funding acquisition. Willem Vercruysse: Methodology (supercapacitors), Validation, Writing - original draft, Writing - review and editing. Dries Vandamme: Methodology (supercapacitors), Writing - original draft, Writing - review and editing. Hamid Hamed: Methodology (supercapacitors and battery testing), Validation, Writing - original draft, Writing - review and editing. Mohammadhosein Safari: Methodology (supercapacitors and battery testing), Validation, Writing - original draft, Writing - review and editing. Elien Derveaux: Methodology (NMR), Validation, Investigation, Writing - original draft, Writing - review and editing. Peter Adriaensens: Methodology (NMR), Validation, Investigation, Writing - original draft, Writing - review and editing. Marlies K. Van Bael: Resources, Writing - original draft, Writing - review and editing, Supervision, Funding acquisition, Project administration. An Hardy: Conceptualization, Resources, Writing - original draft, Writing - review and editing, Supervision, Funding acquisition, Project administration.

### Notes

The authors declare no competing financial interest.

## ■ ACKNOWLEDGMENTS

The authors acknowledge the Research Foundation Flanders (FWO Vlaanderen) for financial support under the project number G053519N. Research Foundation Flanders (FWO Vlaanderen) and Hasselt University are acknowledged for the financial support of this research via the Hercules project AUHL/15/2-GOH3816N. The authors thank Gunter Reekmans for his help with the NMR measurements and the interpretation of the data. Further, the authors thank Younas Verhille for electrode preparation.

## ■ REFERENCES

(1) Pan, H.; Hu, Y.-S.; Chen, L. Room-Temperature Stationary Sodium-Ion Batteries for Large-Scale Electric Energy Storage †. *Energy Environ. Sci.* **2013**, *6*, 2338.

(2) Li, F.; Wei, Z.; Manthiram, A.; Feng, Y.; Ma, J.; Mai, L. Sodium-Based Batteries: From Critical Materials to Battery Systems. *J. Mater. Chem. A Mater.* **2019**, *7* (16), 9406−9431.

(3) Chayambuka, K.; Mulder, G.; Danilov, D. L.; Notten, P. H. L.; Chayambuka, K.; Mulder Vito, G.; Danilov, D. L.; L Notten, P. H. Sodium-Ion Battery Materials and Electrochemical Properties Reviewed. *Adv. Energy Mater.* **2018**, *8* (16), 1800079.

(4) Slater, M. D.; Kim, D.; Lee, E.; Johnson, C. S. Sodium-Ion Batteries. *Adv. Funct. Mater.* **2013**, *23* (8), 947−958.

(5) Yabuuchi, N.; Kubota, K.; Dahbi, M.; Komaba, S. Research Development on Sodium-Ion Batteries. *Chem. Rev.* **2014**, *114* (23), 11636−11682.

(6) Kubota, K.; Komaba, S. Review-Practical Issues and Future Perspective for Na-Ion Batteries. *J. Electrochem. Soc.* **2015**, *162* (14), A2538−A2550.

(7) Li, L.; Zheng, Y.; Zhang, S.; Yang, J.; Shao, Z.; Guo, Z. Recent Progress on Sodium Ion Batteries: Potential High-Performance Anodes. *Energy Environ. Sci.* **2018**, *11* (9), 2310−2340.

(8) Eshetu, G. G.; Elia, G. A.; Armand, M.; Forsyth, M.; Komaba, S.; Rojo, T.; Passerini, S. Electrolytes and Interphases in Sodium-Based Rechargeable Batteries: Recent Advances and Perspectives. *Adv. Energy Mater.* **2020**, *10* (20), 2000093.
(9) Yan, G.; Mariyappan, S.; Rousse, G.; Jacquet, Q.; Deschamps, M.; David, R.; Mirvaux, B.; Freeland, J. W.; Tarascon, J.-M. Higher Energy and Safer Sodium Ion Batteries via an Electrochemically Made Disordered Na3V2(PO4)2F3Material. *Nat. Commun.* **2019**, *10* (1), 585.
(10) Monti, D.; Jó, E.; Boschin, A.; Palací, M. R.; Ponrouch, A.; Johansson, P. Towards Standard Electrolytes for Sodium-Ion Batteries: Physical Properties, Ion Solvation and Ion-Pairing in Alkyl Carbonate Solvents. *Phys. Chem. Chem. Phys.* **2276**, *22*, 22768.
(11) Ponrouch, A.; Marchante, E.; Courty, M.; Tarascon, J. M.; Palacín, M. R. In Search of an Optimized Electrolyte for Na-Ion Batteries. *Energy Environ. Sci.* **2012**, *5* (9), 8572−8583.
(12) Zhu, C.; Wu, D.; Wang, C.; Ma, J. Flame-Retardant, Self-Purging, High-Voltage Electrolyte for Safe and Long-Cycling Sodium Metal Batteries. *Adv. Funct. Mater.* **2024**, 2406764.
(13) Liang, H. J.; Liu, H. H.; Guo, J. Z.; Zhao, X. X.; Gu, Z. Y.; Yang, J. L.; Zhang, X. Y.; Liu, Z. M.; Li, W. L.; Wu, X. L. Self-purification and silicon-rich interphase achieves high-temperature (70°C) sodium-ion batteries with nonflammable electrolyte. *Energy Storage Mater.* **2024**, *66*, 103230.
(14) Uhl, M.; Geng, T.; Schuster, P. A.; Schick, B. W.; Kruck, M.; Fuoss, A.; Kuehne, A. J. C.; Jacob, T. Combining Deep Eutectic Solvents with TEMPO-Based Polymer Electrodes: Influence of Molar Ratio on Electrode Performance. *Angew. Chem., Int. Ed.* **2023**, *62* (2), No. e202214927.
(15) Uhl, M.; Sadeeda, S.; Penert, P.; Schuster, P. A.; Schick, B. W.; Muench, S.; Farkas, A.; Schubert, U. S.; Esser, B.; Kuehne, A. J. C.; Jacob, T.; Uhl, M.; Schick, B. W.; Farkas, A.; Jacob, T.; Penert, P.; Esser, B.; Schuster, P.; C Kuehne, A. J.; Muench, S.; Schubert, U. S. All-Organic Battery Based on Deep Eutectic Solvent and Redox-Active Polymers. *ChemSusChem* **2023**, *17* (1), No. e202301057.
(16) Liu, K.; Wang, Z.; Shi, L.; Jungsuttiwong, S.; Yuan, S. Ionic Liquids for High Performance Lithium Metal Batteries. *J. Energy Chem.* **2021**, *59*, 320−333.
(17) Chatterjee, K.; Pathak, A. D.; Lakma, A.; Sharma, C. S.; Sahu, K. K.; Singh, A. K. Synthesis, Characterization and Application of a Non-Flammable Dicationic Ionic Liquid in Lithium-Ion Battery as Electrolyte Additive. *Sci. Rep.* **2020**, *10* (1), 9606.
(18) Guo, J. Z.; Gu, Z. Y.; Du, M.; Zhao, X. X.; Wang, X. T.; Wu, X. L. Emerging Characterization Techniques for Delving Polyanion-Type Cathode Materials of Sodium-Ion Batteries. *Mater. Today* **2023**, *66*, 221−244.
(19) Huang, Z. X.; Gu, Z. Y.; Heng, Y. L.; Huixiang Ang, E.; Geng, H. B.; Wu, X. L. Advanced Layered Oxide Cathodes for Sodium/Potassium-Ion Batteries: Development, Challenges and Prospects. *Chem. Eng. J.* **2023**, *452*, 139438.
(20) Gu, Z. Y.; Wang, X. T.; Heng, Y. L.; Zhang, K. Y.; Liang, H. J.; Yang, J. L.; Ang, E. H.; Wang, P. F.; You, Y.; Du, F.; Wu, X. L. Prospects and Perspectives on Advanced Materials for Sodium-Ion Batteries. *Sci. Bull.* **2023**, *68*, 2302−2306.
(21) De Sloovere, D.; Vanpoucke, D. E. P.; Paulus, A.; Joos, B.; Calvi, L.; Vranken, T.; Reekmans, G.; Adriaensens, P.; Eshraghi, N.; Mahmoud, A.; Boschini, F.; Safari, M.; Van Bael, M. K.; Hardy, A. Deep Eutectic Solvents as Nonflammable Electrolytes for Durable Sodium-Ion Batteries. *Adv. Energy Sustainability Res.* **2022**, *3* (3), 2100159.
(22) Xiong, W.; Zhang, X.; Tu, Z.; Hu, X.; Wu, Y. Novel Deep Eutectic Electrolyte Induced by Na···N Interactions for Sodium Batteries. *Ind. Eng. Chem. Res.* **2023**, *62* (1), 51−61.
(23) Chen, J.; Yang, Z.; Xu, X.; Qiao, Y.; Zhou, Z.; Hao, Z.; Chen, X.; Liu, Y.; Wu, X.; Zhou, X.; Li, L.; Chou, S. Non-Flammable Succinonitrile-Based Deep Eutectic Electrolyte for Intrinsically Safe High-Voltage Sodium-Ion Batteries. *Adv. Mater.* **2024**, *36* (28), 2400169.
(24) Liu, T.; Wu, H.; Du, X.; Wang, J.; Chen, Z.; Wang, H.; Sun, J.; Zhang, J.; Niu, J.; Yao, L.; Zhao, J.; Cui, G. Water-Locked Eutectic Electrolyte Enables Long-Cycling Aqueous Sodium-Ion Batteries. *ACS Appl. Mater. Interfaces* **2022**, *14* (29), 33041−33051.
(25) Myshakina, N. S.; Ahmed, Z.; Asher, S. A. Dependence of Amide Vibrations on Hydrogen Bonding. *J. Phys. Chem. B* **2008**, *112* (38), 11873−11877.
(26) Miyazawa, T.; Shimanouchi, T.; Muzushima, S. I. Normal Vibrations of N-Methylacetamide. *J. Chem. Phys.* **2004**, *29* (3), 611.
(27) Huang, J.; Hollenkamp, A. F. Thermal Behavior of Ionic Liquids Containing the FSI Anion and the $Li^+$ Cation. *J. Phys. Chem. C* **2010**, *114* (49), 21840−21847.
(28) Matsumoto, K.; Oka, T.; Nohira, T.; Hagiwara, R. Polymorphism of Alkali Bis(Fluorosulfonyl)Amides ($M[N(SO_2F)_2]$, M = Na, K, and Cs). *Inorg. Chem.* **2013**, *52* (2), 568−576.
(29) Kerner, M.; Plylahan, N.; Scheers, J.; Johansson, P. Ionic Liquid Based Lithium Battery Electrolytes: Fundamental Benefits of Utilising Both TFSI and FSI Anions? *Phys. Chem. Chem. Phys.* **2015**, *17* (29), 19569−19581.
(30) Forsyth, M.; Yoon, H.; Chen, F.; Zhu, H.; MacFarlane, D. R.; Armand, M.; Howlett, P. C. Novel Na+ Ion Diffusion Mechanism in Mixed Organic-Inorganic Ionic Liquid Electrolyte Leading to High Na+ Transference Number and Stable, High Rate Electrochemical Cycling of Sodium Cells. *J. Phys. Chem. C* **2016**, *120* (8), 4276−4286.
(31) Joos, B.; Vranken, T.; Marchal, W.; Safari, M.; Van Bael, M. K.; Hardy, A. T. Eutectogels: A New Class of Solid Composite Electrolytes for Li/Li-Ion Batteries. *Chem. Mater.* **2018**, *30* (3), 655−662.
(32) Guo, M.; Liu, C.; Zhang, Z.; Zhou, J.; Tang, Y.; Luo, S.; Guo, M.; Liu, C.; Luo, S.; Zhang, Z.; Zhou, J.; Tang, Y. Flexible $Ti_3C_2Tx$@Al electrodes with Ultrahigh Areal Capacitance: In Situ Regulation of Interlayer Conductivity and Spacing. *Adv. Funct. Mater.* **2018**, *28*, 1803196.
(33) Dong, L.; Xu, C.; Yang, Q.; Fang, J.; Li, Y.; Kang, F. High-Performance Compressible Supercapacitors Based on Functionally Synergic Multiscale Carbon Composite Textiles. *J. Mater. Chem. A Mater.* **2015**, *3* (8), 4729−4737.
(34) Tran, K. T. T.; Le, L. T. M.; Phan, A. L. B.; Tran, P. H.; Vo, T. D.; Truong, T. T. T.; Nguyen, N. T. B.; Garg, A.; Le, P. M. L.; Tran, M. V. New Deep Eutectic Solvents Based on Ethylene Glycol - LiTFSI and Their Application as an Electrolyte in Electrochemical Double Layer Capacitor (EDLC). *J. Mol. Liq.* **2020**, *320*, 114495.
(35) Phadke, S.; Amara, S.; Anouti, M. Gas Evolution in Activated-Carbon-Based Supercapacitors with Protic Deep Eutectic Solvent as Electrolyte. *ChemPhysChem* **2017**, *18* (17), 2364−2373.
(36) Ochai-Ejeh, F. O.; Madito, M. J.; Momodu, D. Y.; Khaleed, A. A.; Olaniyan, O.; Manyala, N. High Performance Hybrid Supercapacitor Device Based on Cobalt Manganese Layered Double Hydroxide and Activated Carbon Derived from Cork (Quercus Suber). *Electrochim. Acta* **2017**, *252*, 41−54.
(37) Kavil, J.; Anjana, P. M.; Periyat, P.; Rakhi, R. B. Titania Nanotubes Dispersed Graphitic Carbon Nitride Nanosheets as Efficient Electrode Materials for Supercapacitors. *J. Mater. Sci.: Mater. Electron.* **2018**, *29* (19), 16598−16608.
(38) Chidiac, J.; Nikiforidis, G.; Timperman, L.; Anouti, M. Non-Flammable Sodium Asymmetric Imide Salt-Based Deep Eutectic Solvent for Supercapacitor Applications. *ChemPhysChem* **2022**, *23* (19), No. e202200224.
(39) Zaidi, W.; Timperman, L.; Anouti, M. Deep Eutectic Solvent Based on Sodium Cations as an Electrolyte for Supercapacitor Application. *RSC Adv.* **2014**, *4* (86), 45647−45652.
(40) Peng, J.; Zhang, W.; Liu, Q.; Wang, J.; Chou, S.; Liu, H.; Dou, S. Prussian Blue Analogues for Sodium-Ion Batteries: Past, Present, and Future. *Adv. Mater.* **2022**, *34* (15), 2108384.
(41) Yan, G.; Reeves, K.; Foix, D.; Li, Z.; Cometto, C.; Mariyappan, S.; Salanne, M.; Tarascon, J.-M. A New Electrolyte Formulation for Securing High Temperature Cycling and Storage Performances of Na-Ion Batteries. *Adv. Energy Mater.* **2019**, *9*, 1901431.


https://doi.org/10.1021/acsomega.4c02896
*ACS Omega* 2024, 9, 42343−42352

(42) Hou, Q.; Li, P.; Qi, Y.; Wang, Y.; Huang, M.; Shen, C.; Xiang, H.; Li, N.; Xie, K. Temperature-Responsive Solvation of Deep Eutectic Electrolyte Enabling Mesocarbon Microbead Anode for High-Temperature Li-Ion Batteries. *ACS Energy Lett.* **2023**, *8* (9), 3649−3657.



https://doi.org/10.1021/acsomega.4c02896
*ACS Omega* 2024, 9, 42343−42352